CrossMark

MULTIPHASE FLOWS IN MATERIALS PROCESSING

Control of Two-Phase Flows During Startup Operations of Casting Sequences in a Billet Tundish

R.D. MORALES,[1,5] JAVIER GUARNEROS,[2] A. NÁJERA-BASTIDA,[3]
and JAFETH RODRÍGUEZ[4]

1.—Department of Metallurgy and Materials Engineering, Instituto Politécnico Nacional-ESIQIE,
Ed. 7, Zacatenco, 07738 Mexico City, Mexico. 2.—K&E Technologies, Manizales 88, San Pedro
Zacatenco, 07365 Mexico City, Mexico. 3.—Department of Extractive Metallurgy, Instituto Poli-
técnico Nacional, UPIIZ, Blvd, del Bote 022, Cerro del Gato, 98160 Zacatecas, Mexico. 4.—Fac-
ultad de Ingeniería, Universidad Autónoma de Coahuila, Blvd. Fundadores Km 13, Ciudad
Universitaria, 25350 Arteaga, Coahuila, Mexico. 5.—e-mail: rmorales@ipn.mx

The startup operations of continuous casting sequences of steel in a 4-strand
tundish, using three different turbulence inhibitors (TI), were investigated
using a 1/3-scale water model in combination with numerical simulations
through the volume of fluid model. The two-phase flow water–air is used to
model the system, and the liquid steel–air and the liquid–gas interfaces are
tracked by a donor–acceptor principle applied in the computational mesh. In
the actual caster, one of the inhibitors releases the liquid steel with a sensible
heat high enough to avoid freezing in the regions near the outer strands
during the startup of the casting sequence. A second inhibitor improves the
fluid flow control by yielding higher plug flow volume fractions. However, it
promotes steel freezing in the outer strands. The analysis of the results lead to
the design of the third TI with intermediate capability to control the steel flow,
preventing steel freezing in the regions near the outer strands.

INTRODUCTION

Tundish design consists of the reorientation and
guiding of the steel flow to control its turbulence, to
decrease stagnant zones and to float out inclusions.
All flow control systems consist of different arrange-
ments of flow modifiers, such as dams and weirs,
turbulence inhibitors (TI) and a combination of all
these devices.[1] The proper combination of flow mod-
ifiers inside the tundish allows the reorientation of
the steel flow in order to have better control, increase
plug flow volume fractions, while minimizing dead or
stagnant regions.[2] This latter requirement is impor-
tant to avoid the formation of steel skulls in the
corners of the tundish, thus facilitating the stripping
of the residual steel at the end of a casting sequence.
The general procedure to design flow control systems
for tundish operations is based on water modeling, by
determining the residence time distributions (RTD)
curves of pulse-injected tracers in the inlet and either
complemented or not with mathematical simula-
tions.[3,4] There is a trend in the industry to build a
design on the assumption that the tundish is always

operating under steady-state conditions, which is
true during a large fraction of the casting time of a
steel ladle, which explains the great success of the
water and mathematical modeling approaches
employed for these purposes.

Few reports on this topic are related to designs of flow
control systems during unsteady-state operations as
reported by some researchers, specifically during ladle
changes.[5,6] Other important unsteady-state operation
of the tundish is the starting up of casting sequences,
especially when steel splashing becomes a safety issue
in the casting floor. It is important to remark that fluid
flow control during steady-state operations generally
do not match the flow control requirements during
unsteady-state operations. A specific case related to the
above statement has been analyzed, and is presented in
the next section.

PRESENTATION OF THE PROJECT

Figure 1a, b, and c corresponds to a 1/3-scale
billet tundish of a 4-strand machine. The steady-
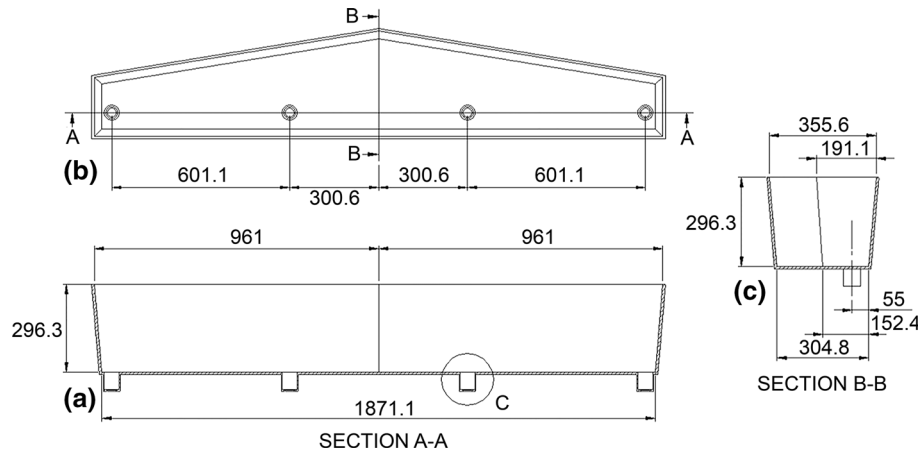state and the unsteady-state filling operations of

Fig. 1. Dimensions of the billet tundish at 1/3-scale: (a) frontal view, (b) plant view, and (c) lateral view.

Table I. Operating conditions of the tundish (1/3-scale) under unsteady conditions (startup of a casting sequence)

Flow parameters	TI1
Normal operating level	254 mm
Ladle shroud: inside diameter	25 mm
Ladle Shroud: submergence	161 mm
Typical liquid flow rate at inlet	19.92 l/min
Flow rate for tundish filling	40 l/min
Inside diameter of the strand	18 mm

this tundish are summarized in Table I. Liquid steel splashing and spreading at the start of the casting sequence, and liquid steel flow control through this tundish is performed using a turbulence inhibitor with the geometric characteristics shown in Fig. 2a. The reports of the operators indicated that this TI1 performs quite well, as steel splashing is minimized, steel freezing in the outer strands during startups of casting sequences is prevented and steel cleanliness improved. However, the management decided to improve the capacity of the tundish to float out inclusions, and a new TI (TI2; Fig. 2b) was designed. The flow patterns yielded by this inhibitor indicated that this was the case, i.e., a higher fraction of plug flow and a smaller dead volume fraction were reported. However, during the industrial trials using the TI2, some of the heat presented early steel freezing in the outer strands. It was thought that the root cause of the steel freezing was the porous plug of the ladle not being free enough of debris, thereby impeding the argon flow to sufficiently stir the liquid steel during those trials. With further trials, it was concluded that, even if TI2 provided better flow control parameters, it had an unacceptable performance during the startup oper-

ations of casting sequences, as the steel freezing persisted even with the same preheating tundish practices and similar steel superheats. It was then concluded that the TI1 delivered a larger amount of steel to the outer strands with a faster speed, while decreasing energy losses without steel freezing problems. The objective was then switched to avoid steel freezing in the outer strands, while maintaining, as much as possible, the good capacity to float out inclusions. The available modern tools, such as the multiphase simulation and physical modeling approaches, increase the capabilities to find a proper solution to this problem.

EXPERIMENTAL DESCRIPTION

The first step in this project is to characterize the flow patterns of liquid steel in this tundish using the proven techniques of water modeling through pulse injections of a red dye tracer in the entry jet, in order to obtain the residence time distributions curves[2] in the inner and outer strands. A 1/3-scale model of the tundish, made of transparent plastic, 12 mm thick, was built with the dimensions shown in Fig. 1a, b, and c. The inhibitors, TI1 and TI2, were built using 3D-printing technologies. The tracer, with a specified concentration, was injected through a syringe in the ladle shroud, and the mix was monitored in the inner and outer strands. The water samples were pumped, by peristaltic pumps, to a pair of colorimeters to measure the concentrations of the tracer at different times. The signals of these apparatuses were fed into a computer equipped with an acquisition card to plot in real time the RTD curves required to carry on the flow analysis. This model was also employed to study the startups of casting sequences under the operating conditions given in Table I. A third TI (TI3) was designed (and 3D-printed) and put through several iterations between the water model and mathematical models, as explained below.
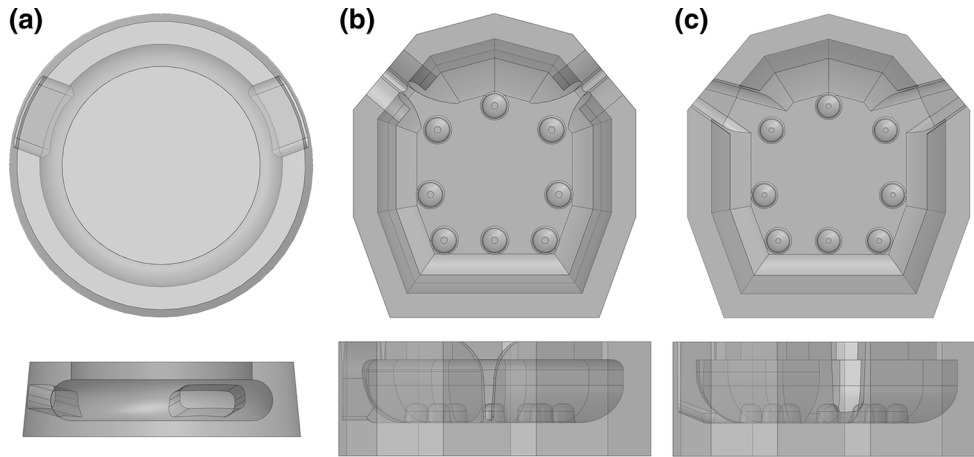
Fig. 2. Geometries of the turbulence inhibitors: (a) TI1, (b) TI2, and (c) TI3.

MATHEMATICAL TWO-PHASE MODEL

The mathematical simulations in this study were focused on the starting up of the casting sequence to examine the liquid splashing and fluid dynamics of the initial tundish-filling process. The objective of these simulations was then to track the gas–liquid interfaces during the initial conditions of turbulence and the interaction of the liquid and air with the TI at the first instances of the tundish filling. Given the interest outlined here, the most appropriate computing scheme is the volume of fluid model (VOF).[7] In this model, there are continuity equations for each phase and a single momentum transfer equation for all the phases. The VOF model is based on a scalar function indicator with magnitudes between zero and unity to distinguish between two different fluids. It is given by the volume fraction occupying one of the fluids within the volume V and is denoted conventionally in a discrete form:

$$\alpha_q = \lim_{V \to 0} \frac{1}{V} \int \int \int \alpha_q(x, y, zt) \mathrm{d}V \qquad (1)$$

A value of zero indicates the presence of one fluid and a value of unity indicates the second fluid. On a computational mesh, volume fraction values between these two limits indicate the presence of the interface, and the value provides an indication of the relative proportions occupying the cell volume. The physical properties of the fluids are estimated by simple additive rules,

$$\rho_m = \sum_{q=1}^{2} \alpha_q \rho_q \quad \mu_m = \sum_{q=1}^{2} \alpha_q \mu_q \qquad (2)$$

The continuity equation (without mass exchange between the phases) is:

$$\frac{\partial \alpha_q}{\partial t} + \nabla \cdot (\alpha_q v_q) = 0 \qquad (3)$$

The velocity–momentum fields, shared by the two phases, is:

$$\frac{\partial(\rho v)}{\partial t} + \nabla \cdot (\rho v v) = -\nabla p + \nabla \cdot \left[\mu(\nabla v + \nabla v^{\mathrm{T}}) \right] + \rho g + F \qquad (4)$$

The physical properties are those calculated through Eq. 2 and, consequently, the volume fraction of the phases is implicit in Eq. 4. To define the interfaces between the two phases, the donor–acceptor formulation of the VOF model is adopted.[8] The tracking of the interfaces between the two phases is carried out by solving the equation of continuity through an explicit scheme setting a Courant number of 0.5:

$$\frac{\alpha_q^{n+1} \rho_q^{n+1} + \alpha_q^n \rho_q^n}{\Delta t} + \sum_f \left(\rho_q^{n+1} v_q^{n+1} \alpha_{qf}^{n+1} \right) = 0 \qquad (5)$$

The contribution of turbulent stresses to the momentum equation is given by the term $(\nabla \cdot \nabla v^{\mathrm{T}})$, in Eq. 4. Therefore, one of the appropriate models to close Eqs. 3 and 4 is obtained through the realizable k–ε model.[9] Two additional equations for the turbulent kinetic energy and the dissipation rate of the kinetic energy form part of the system of equations to be solved.[8,9] The finite volume method was used for the discretization of these equations,[10] building a non-structured mesh composed mostly of tetrahedral cells.

Boundary Conditions and Algorithm of Solution

At the solid surfaces of the tundish system, the logarithmic wall function[8] is employed to link the flow field out of the boundary layer with the velocities, close to the wall, inside this layer. In the inlet, inside the ladle shroud, a turbulent velocity profile is assumed through the 1/7th law of turbulent flows in

pipes.[11] Outlet velocities were also used as boundary conditions in the four strands of the tundish. A pressure condition is applied in the bath surface. The PISO algorithm[12] is employed to solve the set of Eqs. 3 and 4. At the water–air interfaces, the surface tension force is substituted as a momentum source in the last term (right side of Eq. 4), designated by the letter F. The computing of this force was performed through the continuum surface model of Brackbill.[13] The physical properties used in the model for water density, water viscosity and surface tension are 1000 kg m^{-3}, 0.001 Pa s, and 0.073 N m^{-1}, respectively. Air density and air viscosity are 1.2 kg m^{-3} and 18.27 $\times$ 10^{-6} Pa s, respectively.[5,6]

Redesign Methodology for the TI2

It was decided to maintain the same type of design of the inhibitor TI2, and various simulations with different configurations using the two-phase model presented above were performed to obtain a similar amount of steel delivered to the outer strands, with the same flowing speed as the one observed when using the inhibitor T1. Back and forth iterations from water modeling to mathematical simulations, as mentioned above, allowed the attainment of a final suitable design, which is shown in Fig. 2c.

RESULTS AND DISCUSSION

Figure 3 shows the averaged RTD curves considering the inner and outer strands in the three inhibitors. Table II shows the experimental parameters determined through the tracer experiments and an outline of the method employed for the treatment of the averaging RTD data. As seen in Table II, TI2 yields the highest flow volume fractions under plug flow patterns. Comparing TI1 and TI3, there is an improvement of the flow
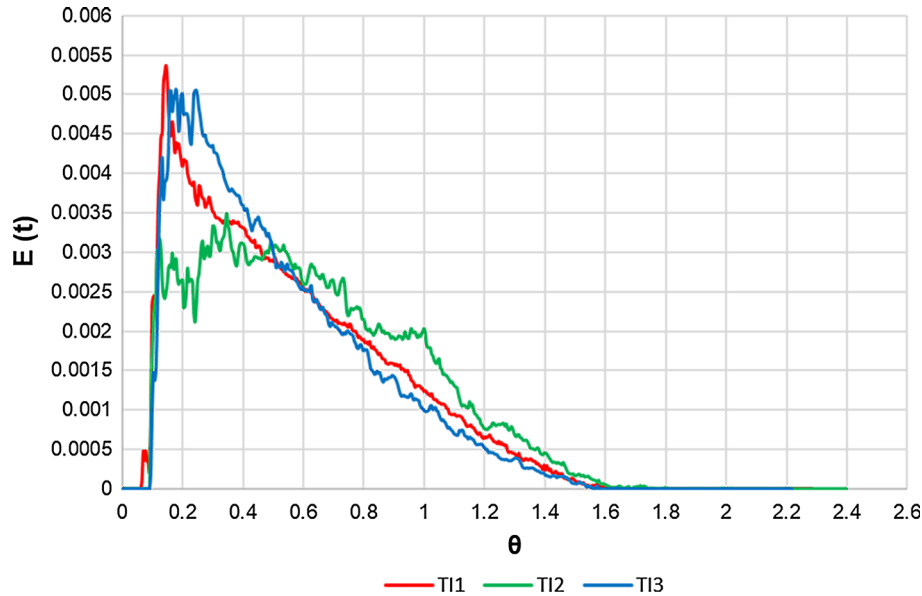

Fig. 3. Averaged residence time distribution curves, including inner and outer strands, of fluid flow in the tundish using different turbulence inhibitors.

Table II. Experimental averaged flow parameters from the RTD curves

Flow parameters	TI1	TI2	TI3
Average times (s)	358.4337	358.4337	358.4337
Plug (%)	0.0816	0.1695	0.1088
Mixture (%)	0.4590	0.4835	0.4055
Dead volume (%)	0.4594	0.3470	0.4857
C_{peak} (g/cm^3)	26.37E−06	27.13E−06	32.10E−06

RTD curves
$$E(\tau) = \frac{C_i(t)}{\int C_i(t)dt + \int C_j(t)dt} + \frac{C_j(t)}{\int C_i(t)dt + \int C_j(t)dt}.$$

$$t = \frac{V}{Q}\left(\frac{\text{water volume}}{\text{water flow rate}}\right), \theta_{plug} = \frac{t_{min}}{t} = \frac{V_{plug}}{V}, \frac{V_{plug}}{V} + \frac{V_{mix}}{V} + \frac{V_{dead}}{V} = 1.$$

$$\theta = \frac{t}{t}, \frac{V_d}{V} = 1 - \theta_{mean}, t_{mean} = \frac{\int ct\,dt}{\int c\,dt}.$$
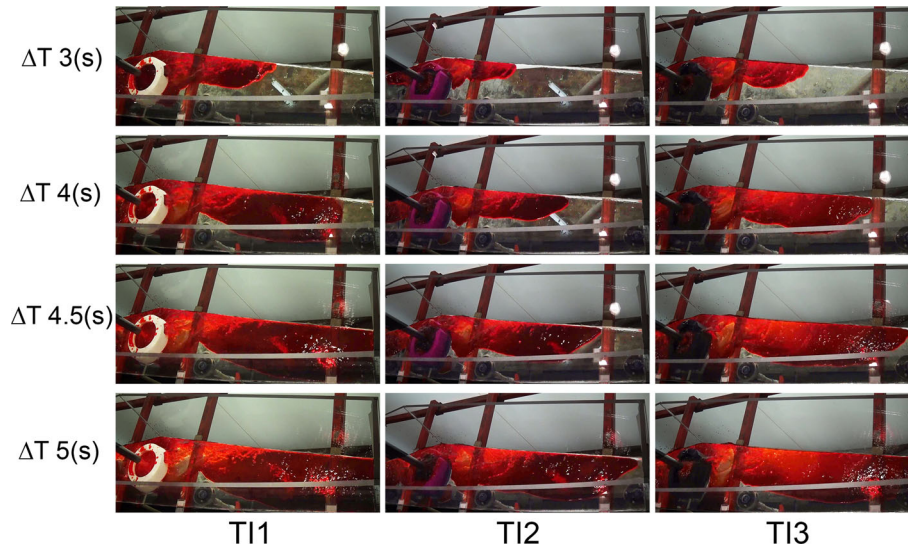
Fig. 4. Experimental displacements of the initial fronts of the liquid streams on the tundish floor at the startup of casting sequence operations modeled with colored red water at different times using inhibitors TI1, TI2, and TI3 (Color figure online).
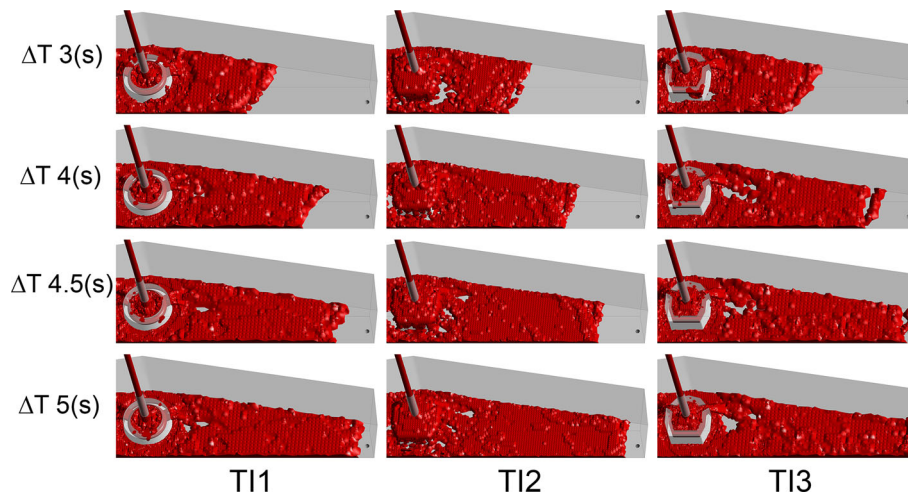

Fig. 5. Computed displacements of the initial fronts of the liquid streams on the tundish floor at the startup of casting sequence operations simulated with VOF model at different times using inhibitors TI1, TI2, and TI3.

characteristics using the latter. The flow yielded by TI3 is a trade-off between a faster stream during the startup and plug flow availability in steady-state conditions. Indeed, Fig. 4 shows comparisons of the displacements of the streams of water along the tundish floor at different times for the three inhibitors, TI1, TI2 and TI3. It is evident that the first stream of water is faster using TI1 and TI3 than when using TI2. This trend is corroborated by the mathematical simulations of the streams displacements at the same times, as shown in Fig. 4, for the three inhibitors, as seen in Fig. 5. It is important to note in this figure that, while inhibitors TI1 and TI3 drain the liquid well, inhibitor TI2 remains fully filled during the operation, delaying the draining of the liquid. The experimental tracks of the stream-front displacements developed by the three inhibitors were estimated from the video of

the corresponding experiments. The computed tracks of the stream-front displacements for each inhibitor were extracted from the numerical files. Both types of data for each inhibitor are plotted in Fig. 6a. Again, the results indicate a very good agreement between the computed and experimental positions of the stream-fronts along the tundish floor. The slopes of those curves at each position give the instantaneous track speeds of the stream-fronts, and it can be seen that, after about 1 s, these speeds are close to zero during a short period of approximately 0.5 s. This is due to the spreading time of the streams on the tundish floor, once they leave the inhibitors. These effects are quite well described by the mathematical model. The streams of liquid steel in the actual tundish will lose less energy if two important premises can be accomplished: The streams have a high speed and their masses are
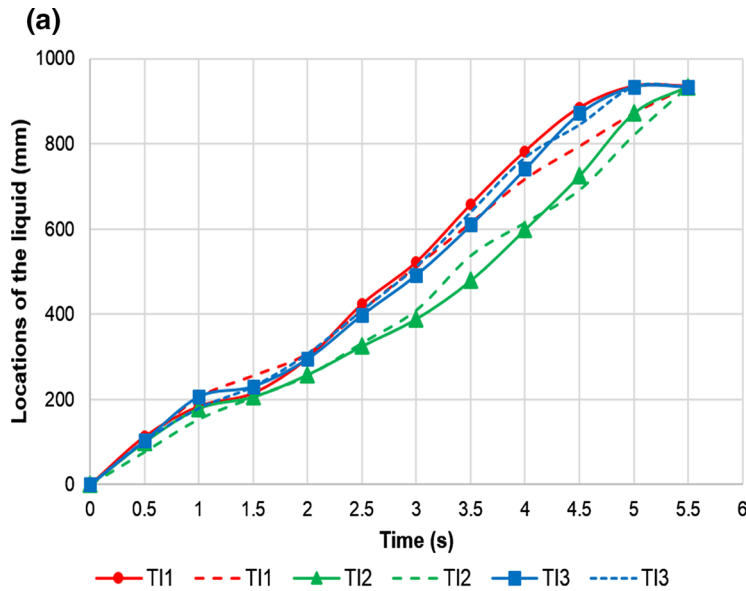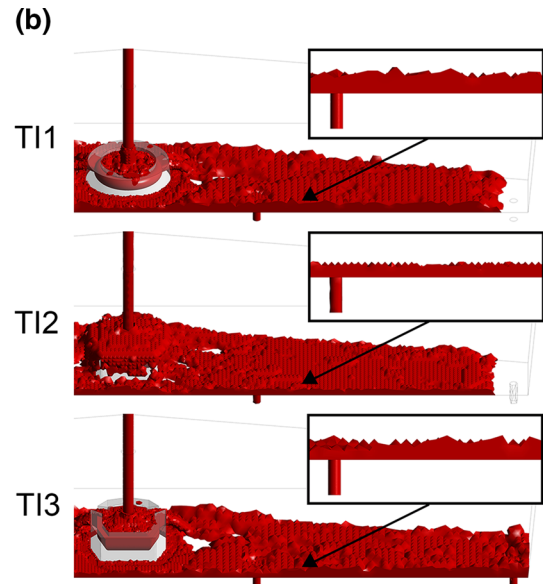
(a)

(b)

Fig. 6. (a) Positions of the liquid streams-fronts along the tundish floor comparing experimental measurements with mathematical simulations using turbulent inhibitors TI1, TI2, and TI3. (b) Thicknesses and free surfaces of the liquid streams at the instant of reaching one of the outer strands.

large enough, so that, at their arrival to the outer strands, this guarantees a liquid with a high sensible heat. To test this hypothesis, the volumes of the computed streams of water, shown in Fig. 5, were calculated through software[14] and their respective volumes were scaled up from 1/3-scale to full-scale. The full-scale volume was multiplied by the density of liquid steel ($7100 \ kg/m^3$), and the results of these operations yielded masses of steel equivalent for half the tundish of the liquid stream of 755.41 kg, 617.09 kg and 762.67 kg for inhibitors TI1, TI2 and TI3, respectively. These results are explicitly presented through the simulated masses of liquid shown in Fig. 6b, in agreement with the results previously presented. The actual tundish is now operating with the inhibitor TI3 without any further report of steel freezing in the outer strands with the usual steel superheats being used in this caster.

CONCLUSION

- The coupling of physical and mathematical multiphase simulations provides a powerful modern approach to solve practical industrial problems.
- The VOF model predicts very well the speed at which the experimental stream of liquid in the tundish flows along the floor.
- The current requirements for the optimum design of turbulence inhibitors include the maximization of plug flow patterns in combination with a good performance during unsteady operations of the tundish.

REFERENCES

1. R.D. Morales, S. López-Ramírez, J. Palafox-Ramos, J. de Barreto Sandoval, and D. Zacharias, *Metall. Mater. Trans. B* 31B, 1505 (2000).
2. H.S. Fogler, *Elements of Chemical Reaction Engineering* (London: Prentice Hall, 1992), pp. 708–795.
3. S. López-Ramírez, J. de Barreto-Sandoval, R.D. Morales, and D. Zacharias, *Metall. Mater. Trans. B* 32B, 615 (2001).
4. A. Espino-Zarate, R.D. Morales, A. Nájera-Bastida, M. Macías-Hernández, and A. Sandoval-Ramos, *Metall. Mater. Trans. B* 41B, 962 (2010).
5. S. García-Hernández, R.D. Morales, J. de Jesús Barreto, I. Calderón-Ramos, and E. Gutiérrez, *Steel Res. Inter.* 86, 517 (2015).
6. R.D. Morales, S. García-Hernández, J. de Barreto-Sandoval, A. Ceballos-Huerta, I. Calderón-Ramos, and E. Gutiérrez, *Metall. Mater. Trans. B* 47B, 2595 (2016).
7. C.W. Hirth and B.D. Nichols, *J. Comput. Phys.* 39, 201 (1981).
8. G.H. Yeoh and J. Tu, *Computational Techniques for Multiphase Flows* (Oxford: Butterworth-Heinemann, 2010), pp. 133–134.
9. Manual of ANSYS-FLUENT, http://www.ansys.com/Products/Fluids/ANSYS-Fluent. Accessed 5 March 2018.
10. H. Ferziger and M. Peric, *Computational Methods for Fluid Dynamics* (Berlin: Springer, 2002), pp. 72–82.
11. E.N. Lightfoot, R.B. Bird, and W.A. Stewart, *Transport Phenomena* (New York: Wiley, 2007), pp. 152–154.
12. R.I. Issa, *J. Comput. Phys.* 62, 40 (1985).
13. J.U. Brackbill, D.B. Kothe, and C. Zemack, *J. Comput. Phys.* 100, 335 (1992).
14. Manual of Solid Works, www.solidworks.com. Accessed 5 March 2018.